



# CHORUS

This is the accepted manuscript made available via CHORUS. The article has been published as:

## Interaction of Phonons and Dirac Fermions on the Surface of $\text{Bi}_{2}\text{Se}_{3}$ : A Strong Kohn Anomaly

Xuetao Zhu, L. Santos, R. Sankar, S. Chikara, C. . Howard, F. C. Chou, C. Chamon, and M. El-Batanouny

Phys. Rev. Lett. **107**, 186102 — Published 26 October 2011

DOI: [10.1103/PhysRevLett.107.186102](https://doi.org/10.1103/PhysRevLett.107.186102)

# Interaction of Phonons and Dirac Fermions on the Surface of $\text{Bi}_2\text{Se}_3$ : A Strong Kohn Anomaly

Xuetao Zhu<sup>1</sup>, L. Santos<sup>2</sup>, R. Sankar<sup>3</sup>, S. Chikara<sup>1</sup>,

C. Howard<sup>1</sup>, F.C. Chou<sup>3</sup>, C. Chamon<sup>1</sup>, M. El-Batanouny<sup>1\*</sup>

<sup>1</sup>*Department of Physics, Boston University, Boston, MA 02215, USA*

<sup>2</sup>*Department of Physics, Harvard University, Cambridge, MA 02138, USA*

<sup>3</sup>*Center of Condensed Matter Sciences, National Taiwan University, Taipei 10617, Taiwan*

(Dated: September 26, 2011)

We report the first measurements of phonon dispersion curves on the (001) surface of the strong three-dimensional topological insulator  $\text{Bi}_2\text{Se}_3$ . The surface phonon measurements were carried out with the aid of coherent helium beam surface scattering techniques. The results reveal a prominent signature of the exotic metallic Dirac fermion quasi-particles, including a strong Kohn anomaly. The signature is manifest in a low energy isotropic convex dispersive surface phonon branch with a frequency maximum of 1.8 THz, and having a V-shaped minimum at approximately  $2\mathbf{k}_F$  that defines the Kohn anomaly. Theoretical analysis attributes this dispersive profile to the renormalization of the surface phonon excitations by the surface Dirac fermions. The contribution of the Dirac fermions to this renormalization is derived in terms of a Coulomb-type perturbation model.

PACS numbers: 63.20.D-, 63.20.K-, 68.35.Ja, 68.49.Bc, 73.20.-r

The recent discovery of the new class of materials coined topological insulators (TIs) [1–5] has attracted much interest and excitement. Strong TIs have exotic metallic surface states protected by time-reversal invariance (TRI). The presence of the metallic boundary is dictated by the recent  $\mathbf{Z}_2$  classification of TRI insulators into an *ordinary* insulator class ( $\mathbf{Z}_2$ -even), including the vacuum, and a *topological* insulator class ( $\mathbf{Z}_2$ -odd). Members of each class can be adiabatically converted to each other, but not into members of the other class [6–8]. Ordinary and topological phases are separated by a topological phase transition, where the bulk gap has to vanish at the transition point. Thus, the ensuing scenario for a strong TI depicts a topological bulk ( $\mathbf{Z}_2$ -odd), embedded in vacuum ( $\mathbf{Z}_2$ -even), a case which demands that the boundary (surface) be gapless. This gives rise to surface states involving massless Dirac fermion quasi-particles (DFQs) having an odd number of Dirac cones in the surface Brillouin zone (SBZ). Moreover, the strong spin-orbit coupling leads to a definite helicity whereby the spin is locked normal to the wavevector of the electronic state. A fundamental constraining feature of such spin-textured surface states is their robustness against spin-independent scattering, an attribute that protects them from backscattering and localization [9, 10].

In this paper we address, experimentally and theoretically, a manifestation of the exotic surface DFQs that has received little attention: their response to surface phonon excitations, namely surface electron-phonon scattering and the ensuing phonon energy renormalization. In this work, we employ elastic and inelastic helium atom surface scattering (HASS) techniques to determine the surface structure and obtain the surface phonon dispersion curves, respectively. It is well established that He atoms are scattered by the oscillations of the surface elec-

tron density about 2-3 Å away from the first atomic layer, and thus HASS is very sensitive to phonon-induced surface charge density (SCD) oscillations, even those induced by subsurface second-layer displacements [11, 12]. Consequently, HASS intensities carry direct information on the SCD oscillations associated with surface phonons and ultimately on the surface electron-phonon (e-p) interaction. HASS, therefore, is an ideal technique to investigate the collective Dirac electron states response to surface lattice excitations.

Because the family of strong TIs  $\text{Bi}_2\text{X}_3$  (X=Se, Te) was found to have a single Dirac cone with a Dirac point at the SBZ center [13–17], it has been the focus of ongoing intense experimental and theoretical studies. Angle- and spin-resolved photoemission spectroscopy measurements provided strong evidence of the existence of the linearly dispersive Dirac cone and the spin texture. Moreover, scanning-tunneling microscopy confirmed the absence of backscattering, namely, scattering between states of opposite momentum and opposite spin [9, 18]. We selected to study  $\text{Bi}_2\text{Se}_3$  because of its simplicity, its relatively wide gap of 300 meV, and the rich trove of information available about its DFQ surface states [19–23].

The (001)  $\text{Bi}_2\text{Se}_3$  crystal surface belongs to the  $p6mm$  two-dimensional space group. The corresponding SBZ is shown in figure 1; with high-symmetry points  $\bar{\Gamma}$ ,  $\bar{M}$  and  $\bar{K}$ . Extensive elastic and inelastic He scattering measurements of the  $\text{Bi}_2\text{Se}_3$ (001) surface were carried out [24]. The processed inelastic data is presented in figure 3 along the  $\bar{\Gamma}$ - $\bar{M}$ ,  $\bar{\Gamma}$ - $\bar{K}$  and  $\bar{K}$ - $\bar{M}$  directions as orange dots together with their respective error bars.

In order to interpret and fit the experimental inelastic data, we carried out phenomenological surface lattice dynamical calculations, based on the pseudo-charge model (PCM) [24–26] and applied to slab geometries contain-

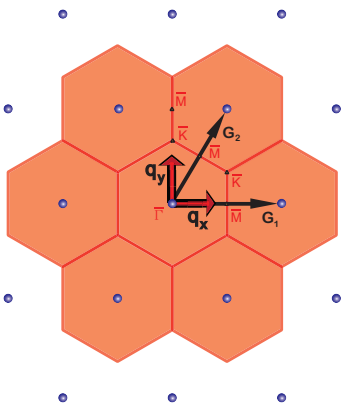


FIG. 1. The extended surface Brillouin zone, showing high-symmetry points  $\bar{\Gamma}$ ,  $\bar{M}$  and  $\bar{K}$ . The  $\bar{\Gamma}$ - $\bar{M}$  direction lies along  $q_x$ , while the  $\bar{\Gamma}$ - $\bar{K}$ - $\bar{M}$  line is traced along  $q_y$ . The  $\mathbf{G}_i$ s are surface reciprocal lattice vectors.

ing 30 quintuples. The physical role of the surface DFQ states in the phonon energy renormalization was subsequently studied with the aid of a microscopic model based on Coulomb-type perturbations. The model was incorporated in calculations of density-density correlations that take into account the helicity and linear dispersion of the surface DFQ states.

The slab calculations were preceded by a bulk calculation [24] based on PCM and fitted to available Raman and IR data [27, 28]. To obtain a best-fit to the measured surface phonon dispersion curves the following changes to bulk parameter values were made: The surface Se-Bi force constant was reduced by 25% from its bulk value; this is a reasonable change since the non-metallic bonding in the two topmost layers is effectively reduced to allow for the emergence of the metallic electrons. A new planar force constant involving surface Se-Se ions was introduced. To account for the metallic deformability of the surface DFQs we reduced the magnitude of the pseudocharge-ion coupling constant  $T_S$  in the topmost pyramid involving Se and Bi from its bulk value  $T_B^1$  by about  $\frac{\Delta T_S}{T_B^1} = \frac{T_B^1 - T_S}{T_B^1} \simeq 13\%$  [24]. Physically,  $\Delta T_S$  accounts for the extra screening provided by the DFQ surface states, which is proportional to the corresponding Fermi surface density of states,  $\mathcal{D}_F \propto E_F \propto k_F$ . Hence  $\Delta T_S \propto k_F$ .

However, to underscore the significance of the experimental results and their interpretation in terms of PCM fitting, we start by presenting in figure 2 the surface phonon dispersions for a model employing the bulk value of the ion-pseudo-charge coupling parameter at the surface, namely  $T_S = T_B^1 = 8.07$  N/m [24]. The calculated surface phonon dispersion curves are presented in figure 2 as black dots, and the colored areas represent the projection of the bulk bands onto the SBZ. The details of those bulk bands are discussed in [24]. The important feature

to be noted is the presence of a surface Rayleigh branch that splits from the edge of the acoustic orange band, extending from  $\omega = 0$  to  $\omega \simeq 3.7$  THz. Its Rayleigh character is also shown in [24].

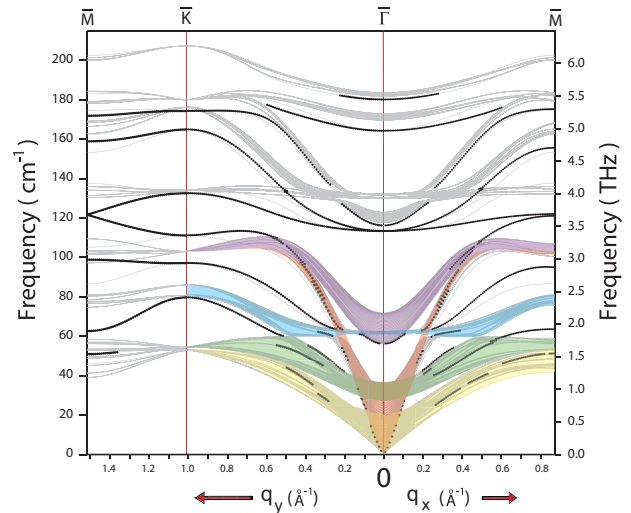


FIG. 2. Calculated surface phonon dispersion curves (black dots) along the  $\bar{\Gamma}$ - $\bar{M}$  and  $\bar{\Gamma}$ - $\bar{K}$  directions, for  $T_S = T_B^1 = 8.07$  N/m, the bulk value. The colored areas represent the projection of the bulk bands onto the SBZ. The details of those bulk bands are discussed in [24].

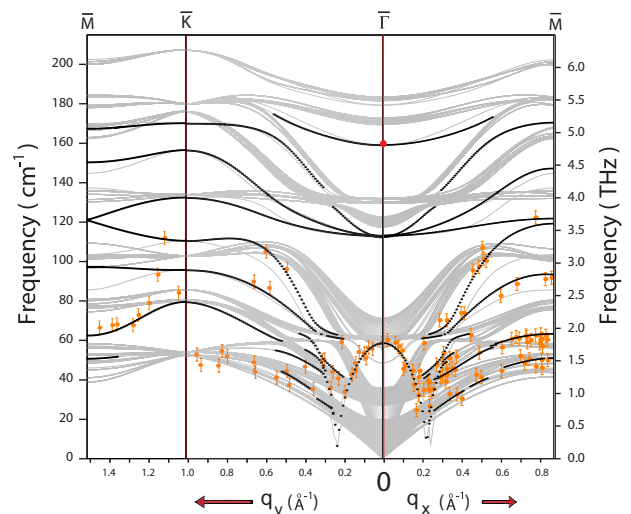


FIG. 3. Surface phonon dispersion curves along the  $\bar{\Gamma}$ - $\bar{M}$  and  $\bar{\Gamma}$ - $\bar{K}$  directions: Experimental data appear as orange dots with error bars reflecting instrument resolution, while the calculated dispersion curves, using PCM with  $T_S = 7.05$  N/m, are represented by black dots. The gray background represents the projection of the bulk bands on the SBZ. The red dot on  $\bar{\Gamma}$  at  $160 \text{ cm}^{-1}$  represents an experimental surface Raman mode reported in Ref.[29].

By contrast, the calculated surface phonon dispersion curves that provide a best-fit for the experimental data,

correspond to a reduced value of  $T_S$  of 7.05 N/m. The calculated surface phonon dispersion curves are shown in figure 3 as black dots, superimposed on the experimental data which is displayed as solid orange dots with error bars. The single red dot at the  $\bar{\Gamma}$ -point, at about 5 THz, is a Raman surface frequency reported in [29].

We shall focus our attention on two important observations regarding figure 3. First, we should discern the absence of a surface Rayleigh branch in both experimental and calculated dispersion curves. Second, we observe the emergence of a “prominent” isotropic parabolic dispersion branch centered at the  $\bar{\Gamma}$ -point with a frequency of 1.8 THz (7.4 meV); the PCM calculations confirm that at  $\bar{\Gamma}$  it has a vertical shear ( $z$ ) polarization, with  $u_{Se}^z/u_{Bi}^z = 2.8$ , where  $u^z$  is the respective ionic displacement. This branch terminates in a V-shaped minimum located at  $q \simeq 0.2 \text{ \AA}^{-1}$ , a value that roughly corresponds to  $2k_F$  of the DFQs, and thus signals the manifestation of a strong Kohn anomaly [30]. The isotropy of this branch and its apparent termination at  $2k_F$  can be explained by a scenario involving the DFQ surface states, in particular their isotropic Fermi surface. In this scenario, the V-shaped feature marks the boundary between an operative DFQ screening for  $q < 2k_F$ , and its suppression above this value, which is a typical signature of a Kohn anomaly. Lattice dynamics calculations reveal some bulk penetration of vertical shear modes for  $q > 2k_F$  reflecting a diminished role of DFQ screening and more compatibility with the insulating bulk. We shall establish below the intimate link between the dispersive character of this branch and the surface DFQ states response to ionic displacements. The polarization and other properties of the remaining surface phonon dispersive branches are discussed in [24].

We now briefly describe the microscopic model used to study the contributions of the surface Dirac electronic states that define the dispersive character of the prominent phonon branch. Our experimental results demonstrate that this surface phonon branch is “optical” in nature, and thus should be derived from a Coulomb-type perturbative mechanism. Consequently, we construct a perturbative Hamiltonian describing the interaction of the surface Dirac electrons with the electric field resulting from ionic displacements, namely, a linear coupling of the lattice ionic displacement to the DFQ density of the form

$$\mathcal{H}_{\text{el-ph}} = \int d^2\mathbf{r} \rho_{\text{el}}(\mathbf{r}) \sum_{j=1}^N \boldsymbol{\lambda}(\mathbf{r} - \mathbf{R}_j^{(0)}) \cdot \mathbf{u}_j, \quad (1)$$

where  $\rho_{\text{el}}(\mathbf{r})$  is the 2-dimensional electron density, and  $\mathbf{u}_j$  is the displacement of the  $j^{\text{th}}$  surface ion whose equilibrium position is  $\mathbf{R}_j^{(0)}$ .  $\boldsymbol{\lambda}$  is a vector accounting for the position-dependent coupling of the charge density to ionic displacements. As shown in [24], after second quantization, with  $b_{\mathbf{q},\gamma}$  and  $c_{\mathbf{k},\alpha}$  being the annihilation operators

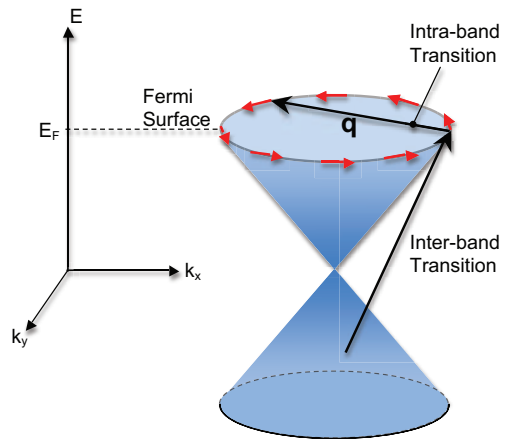


FIG. 4. Intra- and Inter-band transitions of DFQs that contribute to the renormalization of the prominent surface phonon branch.  $\mathbf{q}$  is the phonon wave vector. The red arrows indicate the spin helicity on the Fermi Surface.

for a surface phonon mode  $(\mathbf{q}, \gamma)$  with polarization index  $\gamma$  and an electron with momentum  $\mathbf{k}$  and spin  $\alpha$ , respectively, the Hamiltonian takes the form

$$\mathcal{H}_{\text{el-ph}} = \frac{1}{\sqrt{\mathcal{A}}} \sum_{\alpha=\uparrow,\downarrow} \sum_{\mathbf{k}} g_{\mathbf{q},\gamma} c_{\mathbf{k}+\mathbf{q},\alpha}^\dagger c_{\mathbf{k},\alpha} \hat{A}_{\mathbf{q},\gamma}, \quad (2)$$

where  $\hat{A}_{\mathbf{q},\gamma} \equiv (b_{\mathbf{q},\gamma} + b_{\mathbf{q},\gamma}^\dagger)$ . The electron-phonon coupling constant is

$$g_{\mathbf{q},\gamma} = \sqrt{\frac{N\hbar}{2M\mathcal{A}\omega_{\mathbf{q},\gamma}^{(0)}}} \boldsymbol{\lambda}_{\mathbf{q}} \cdot \hat{\mathbf{e}}_\gamma(\mathbf{q}) \equiv \sqrt{\frac{N\hbar}{2M\mathcal{A}\omega_{\mathbf{q},\gamma}^{(0)}}} \lambda_{\mathbf{q},\gamma}. \quad (3)$$

$\mathcal{A}$  is the surface area,  $N$  the number of primitive cells in  $\mathcal{A}$ ,  $M$  the ionic mass.  $\omega_{\mathbf{q},\gamma}^{(0)}$  is the bare phonon frequency of mode  $(\mathbf{q}, \gamma)$  and  $\hat{\mathbf{e}}_\gamma(\mathbf{q})$  the corresponding polarization vector.  $\boldsymbol{\lambda}_{\mathbf{q}}$  denotes the Fourier transform of  $\boldsymbol{\lambda}(\mathbf{r})$ . A detailed derivation given in [24] leads to the Dyson equation

$$\left(\hbar\omega_{\mathbf{q},\gamma}\right)^2 = \left(\hbar\omega_{\mathbf{q},\gamma}^{(0)}\right)^2 + \frac{\hbar^2}{M\mathfrak{A}} |\lambda_{\mathbf{q}}|^2 \frac{\Pi(\mathbf{q}, \omega_{\mathbf{q},\gamma})}{\varepsilon(\mathbf{q}, \omega_{\mathbf{q},\gamma})}, \quad (4)$$

where  $\omega_{\mathbf{q},\gamma}$  is the renormalized surface phonon frequency, and  $\mathfrak{A}$  is the surface primitive cell area.  $\Pi$  and  $\varepsilon$  are the polarization and dielectric functions in the random phase approximation, respectively, expressed in the helicity basis; the former can be decomposed into two contributions: one due to intra-band and the other due to inter-band excitations as shown in figure 4:

$$\Pi(\mathbf{q}, \omega) = \Pi^{\text{intra}}(\mathbf{q}, \omega) + \Pi^{\text{inter}}(\mathbf{q}, \omega). \quad (5)$$

Explicit expressions for  $\Pi^{\text{intra}}$  and  $\Pi^{\text{inter}}$  are given in [24]. In order to solve (4) self consistently, we need to specify the momentum dependence of the coupling function

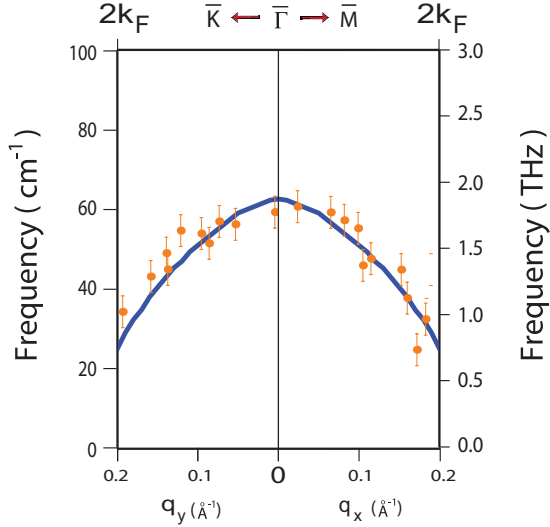


FIG. 5. Renormalized surface topological phonon dispersion curve, superimposed on the corresponding experimental data.

$\lambda_{\mathbf{q},\gamma}$ . We argue that in the range of  $|\mathbf{q}| \leq 2k_F$ , the ionic screened potential  $V(\mathbf{q})$  has very weak dependence on  $q$ , since  $2k_F < q_{\text{TF}} = \frac{e^2 k_F^2}{4\pi\epsilon_0 E_F} = 0.5 \text{ \AA}^{-1}$  the Thomas-Fermi wave vector. Moreover, invoking the sagittal-plane symmetry classification of the surface phonon modes, we specify the general polarization vector of the even parity mode as

$$\hat{\mathbf{e}}_\gamma(\mathbf{q}) \Rightarrow \hat{\mathbf{e}}_\perp(\mathbf{q}) \sim \hat{\mathbf{z}}, \quad \hat{\mathbf{e}}_\parallel(\mathbf{q}) \sim \hat{\mathbf{q}}. \quad (6)$$

$\hat{\mathbf{e}}_\perp(\mathbf{q})$  accounts for the vertical shear component (ionic oscillations in a direction normal to the surface plane) while  $\hat{\mathbf{e}}_\parallel(\mathbf{q})$  is the longitudinal component. The corresponding coupling constant then reads

$$\begin{aligned} \lambda_{\mathbf{q},\gamma} &= \boldsymbol{\lambda}_{\mathbf{q}} \cdot \hat{\mathbf{e}}_\gamma(\mathbf{q}) = \boldsymbol{\lambda}_{\mathbf{q}} \cdot \hat{\mathbf{e}}_\perp(\mathbf{q}) + \boldsymbol{\lambda}_{\mathbf{q}} \cdot \hat{\mathbf{e}}_\parallel(\mathbf{q}) \\ &\equiv \lambda_\perp(\mathbf{q}) + \lambda_\parallel(\mathbf{q}). \end{aligned} \quad (7)$$

In view of the near constancy of  $V(\mathbf{q})$  for  $q \leq 2k_F$ , and the fact that the electron-phonon coupling involves the gradient of the screened potential, we write

$$\boldsymbol{\lambda}_{\mathbf{q}} = \lambda_\perp^{(0)} + \frac{|\mathbf{q}|}{q_0} \lambda_\parallel^{(0)} \quad (8)$$

where  $q_0$  will be appropriately chosen as  $2k_F$ . Notice that at  $\bar{\Gamma}$  ( $\mathbf{q} = \mathbf{0}$ ) the polarization is pure vertical shear, in agreement with the surface symmetry and the PCM.

The Dyson equation now becomes

$$(\hbar\omega_{\mathbf{q},\gamma})^2 = (\hbar\omega_{\mathbf{q},\gamma}^{(0)})^2 + \frac{\hbar^2}{M\mathfrak{A}} (\lambda_\perp)^2 \left( 1 + \frac{|\mathbf{q}|}{k_F} \frac{\lambda_\parallel}{\lambda_\perp} \right) \frac{\Pi(\mathbf{q}, \omega_{\mathbf{q},\gamma})}{\varepsilon(\mathbf{q}, \omega_{\mathbf{q},\gamma})} \quad (9)$$

to first order in  $q$ .

The model depends on two parameters: the bare phonon frequency and the Fermi wave vector. We

identified the former with the experimental value of  $\omega(\mathbf{q} = 0) = 1.8 \text{ THz}$ , where the DFQ response vanishes.  $k_F$  was derived from a sample carrier concentration of  $-1.9 \times 10^{19}/\text{cm}^3$ , obtained from Hall measurements, which correspond to a Fermi energy of about 300 meV and a Fermi wavevector of  $k_F = 0.1 \text{ \AA}^{-1}$ , which is consistent with previous values reported from photoemission measurements [19, 21, 22]. The coupling parameters  $\lambda_\perp^{(0)}$  and  $\lambda_\parallel^{(0)}$  were left as fitting variables. Solutions for  $\omega(\mathbf{q})$  were obtained by carrying out the integrals for  $\Pi(\mathbf{q}, \omega)$ , and solving Eq. (4) iteratively. The calculated best-fit dispersion curve is shown in figure 5, superimposed on the experimental data. The agreement is quite good.

The best fit parameters are

$$\frac{\hbar^2}{M\mathfrak{A}} (\lambda_\perp)^2 = 10^7 \text{ (meV)}^3 \cdot \text{\AA}^2, \quad \frac{\lambda_\parallel}{\lambda_\perp} = 0.65. \quad (10)$$

With  $\frac{\hbar^2}{M\mathfrak{A}} = 4 \times 10^{-3} \text{ meV}$ , we obtain  $\lambda_\perp = 50 \text{ eV} \cdot \text{\AA}$ . This yields a real space value of  $3.4 \text{ eV/\AA}$ , which is quite reasonable since it falls in the range of typical Coulombic interactions.

Finally, we demonstrated above that a TI actually presents a composite system consisting of an “ultra-thin metallic film” and an underlying insulating substrate. As such, the phonons in the metallic film can hardly penetrate into the substrate bulk in order to establish an acoustic Rayleigh branch. However, the unique feature of this system is that for  $q > 2k_F$ , as DFQ screening becomes gradually suppressed, the surface film becomes almost homogeneous with the underlying substrate, and the corresponding modes gradually penetrate into the bulk, ushering the V-shaped dispersion. We designate this unique behavior as a *strong* Kohn anomaly. Moreover, we should emphasize here that theoretical modeling and analysis of the interaction between the surface phonons and the DFQs demonstrate that the linear dispersion and isotropy of the DFQs are responsible for the profile of the prominent surface phonon branch for  $q \leq 2k_F$ .

We should note that some recent studies [31, 32] proposed models based on acoustic-phonon perturbations, derived from the Dirac fermion Hamiltonian, but these perturbations are too weak to account for the observed dispersion.

This work is supported by the U.S. Department of Energy under Grants No. DE-FG02-85ER45222 (MEB) and DEFG02-06ER46316 (CC). FCC acknowledges the support from the National Science Council of Taiwan under project No. NSC 99-2119-M-002-011-MY.

[1] M. Z. Hasan and C. L. Kane, Rev. Mod. Phys. **82**, 3045 (2010).

- [2] X.-L. Qi and S.-C. Zhang, *Rev. Mod. Phys.* (2011).
- [3] J. E. Moore, *Nature* **464**, 194 (2010).
- [4] L. Fu and C. L. Kane, *Phys. Rev. B* **76**, 045302 (2007).
- [5] M. Z. Hasan and J. E. Moore, *Annual Review of Condensed Matter Physics* **2**, 55 (2011).
- [6] C. L. Kane and E. J. Mele, *Phys. Rev. Lett.* **95**, 146802 (2005).
- [7] J. E. Moore and L. Balents, *Phys. Rev. B* **75**, 121306 (2007).
- [8] L. Fu, C. L. Kane, and E. J. Mele, *Phys. Rev. Lett.* **98**, 106803 (2007).
- [9] P. Roushan, J. Seo, C. V. Parker, Y. S. Hor, D. Hsieh, D. Qian, A. Richardella, M. Z. Hasan, R. J. Cava, and A. Yazdani, *Nature* **460**, 1106 (2009).
- [10] T. Zhang, P. Cheng, X. Chen, J.-F. Jia, X. Ma, K. He, L. Wang, H. Zhang, X. Dai, Z. Fang, X. Xie, and Q.-K. Xue, *Phys. Rev. Lett.* **103**, 266803 (2009).
- [11] V. Chis, B. Hellsing, G. Benedek, M. Bernasconi, E. V. Chulkov, and J. P. Toennies, *Phys. Rev. Lett.* **101**, 206102 (2008).
- [12] G. Benedek, M. Bernasconi, V. Chis, E. Chulkov, P. M. Echenique, B. Hellsing, and J. P. Toennies, *J. Phys.: Condens. Matter.* **22**, 084020 (2010).
- [13] Y. L. Chen, J. G. Analytis, J.-H. Chu, Z. K. Liu, S.-K. Mo, X. L. Qi, H. J. Zhang, D. H. Lu, X. Dai, Z. Fang, S. C. Zhang, I. R. Fisher, Z. Hussain, and Z.-X. Shen, *Science* **325**, 178 (2009).
- [14] H.-J. Noh, H. Koh, S.-J. Oh, J.-H. Park, H.-D. Kim, J. D. Rameau, T. Valla, T. E. Kidd, P. D. Johnson, Y. Hu, and Q. Li, *EPL* **81**, 57006 (2008).
- [15] W. Zhang, R. Yu, H.-J. Zhang, X. Dai, and Z. Fang, *New J. Phys.* **12**, 065013 (2010).
- [16] H. Zhang, C.-X. Liu, X.-L. Qi, X. Dai, Z. Fang, and S.-C. Zhang, *Nat. Phys.* **5**, 438 (2009).
- [17] D. Hsieh, Y. Xia, D. Qian, L. Wray, F. Meier, J. H. Dil, J. Osterwalder, L. Patthey, A. V. Fedorov, H. Lin, A. Bansil, D. Grauer, Y. S. Hor, R. J. Cava, and M. Z. Hasan, *Phys. Rev. Lett.* **103**, 146401 (2009).
- [18] K. Park, J. J. Heremans, V. W. Scarola, and D. Minic, *Phys. Rev. Lett.* **105**, 186801 (2010).
- [19] Y. Xia, D. Qian, D. Hsieh, L. Wray, A. Pal, H. Lin, A. Bansil, D. Grauer, Y. S. Hor, R. J. Cava, and M. Z. Hasan, *Nat. Phys.* **5**, 398 (2009).
- [20] J. G. Analytis, J.-H. Chu, Y. Chen, F. Corredor, R. D. McDonald, Z. X. Shen, and I. R. Fisher, *Phys. Rev. B* **81**, 205407 (2010).
- [21] S. R. Park, W. S. Jung, C. Kim, D. J. Song, C. Kim, S. Kimura, K. D. Lee, and N. Hur, *Phys. Rev. B* **81**, 041405 (2010).
- [22] K. Kuroda, M. Arita, K. Miyamoto, M. Ye, J. Jiang, A. Kimura, E. E. Krasovskii, E. V. Chulkov, H. Iwasawa, T. Okuda, K. Shimada, Y. Ueda, H. Namatame, and M. Taniguchi, *Phys. Rev. Lett.* **105**, 076802 (2010).
- [23] O. V. Yazyev, J. E. Moore, and S. G. Louie, *Phys. Rev. Lett.* **105**, 266806 (2010).
- [24] See Supplementary Material at url for details..
- [25] C. S. Jayanthi, H. Bilz, W. Kress, and G. Benedek, *Phys. Rev. Lett.* **59**, 795 (1987).
- [26] C. Kaden, P. Ruggerone, J. P. Toennies, G. Zhang, and G. Benedek, *Phys. Rev. B* **46**, 13509 (1992).
- [27] W. Richter and C. R. Becker, *Phys. Status Solidi (b)* **84**, 619 (1977).
- [28] in *Landolt-Börnstein database - Group III Condensed Matter*, Vol. 41C: Non-Tetrahedrally Bonded Elements and Binary Compounds I, edited by M. S. O. Madelung, U. Rössler (Springer, 2011).
- [29] S. Y. F. Zhao, C. Beekman, L. J. Sandilands, J. E. J. Bashucky, D. Kwok, N. Lee, A. D. LaForge, S. W. Cheong, and K. S. Burch, *Appl. Phys. Lett.* **98**, 141911 (2011).
- [30] W. Kohn, *Phys. Rev. Lett.* **2**, 393 (1959).
- [31] P. Thalmeier, *Phys. Rev. B* **83**, 125314 (2011).
- [32] S. Giraud and R. Egger, *Phys. Rev. B* **83**, 245322 (2011).